Cell Reports

Resource

Optogenetic Control of Nodal Signaling Reveals a Temporal Pattern of Nodal Signaling Regulating Cell Fate Specification during Gastrulation

Graphical Abstract

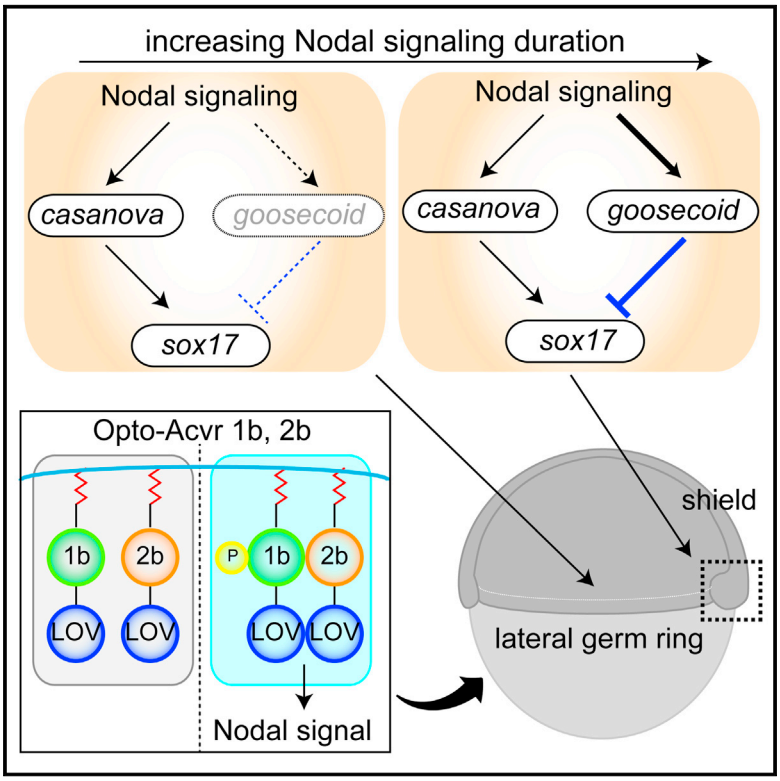

Highlights

- A photoactivatable Nodal receptor spatiotemporally controls Nodal signaling in vivo
- Extended Nodal signaling regulates organizer cell fate specification in zebrafish
- Gsc expression in prechordal plate progenitors suppresses endoderm specification

Authors

Keisuke Sako, Saurabh J. Pradhan, Vanessa Barone, ..., Sanjeev Galande, Harald Janovjak, Carl-Philipp Heisenberg

Correspondence

harald@ist.ac.at (H.J.), heisenberg@ist.ac.at (C.-P.H.)

In Brief

Using a photoactivatable Nodal receptor, Sako et al. find that extending Nodal signaling within the zebrafish embryonic organizer induces prechordal plate and suppresses endoderm specification.

Sako et al., 2016, Cell Reports *16*, 866–877
July 19, 2016 © 2016 The Author(s).
http://dx.doi.org/10.1016/j.celrep.2016.06.036

CellPress

OPEN ACCESS
CellPress

Cell Reports
Resource

Optogenetic Control of Nodal Signaling Reveals a Temporal Pattern of Nodal Signaling Regulating Cell Fate Specification during Gastrulation

Keisuke Sako,[1] Saurabh J. Pradhan,[2] Vanessa Barone,[1] Álvaro Inglés-Prieto,[3] Patrick Müller,[4] Verena Ruprecht,[1] Daniel Čapek,[1] Sanjeev Galande,[2] Harald Janovjak,[3,*] and Carl-Philipp Heisenberg[1,*]
[1]Laboratory of Developmental Biology, Institute of Science and Technology Austria, 3400 Klosterneuburg, Austria
[2]Indian Institute of Science, Education and Research, Pune 411008, India
[3]Laboratory of Synthetic Physiology, Institute of Science and Technology Austria, 3400 Klosterneuburg, Austria
[4]Friedrich Miescher Laboratory of the Max Planck Society, 72076 Tübingen, Germany
*Correspondence: harald@ist.ac.at (H.J.), heisenberg@ist.ac.at (C.-P.H.)
http://dx.doi.org/10.1016/j.celrep.2016.06.036

SUMMARY

During metazoan development, the temporal pattern of morphogen signaling is critical for organizing cell fates in space and time. Yet, tools for temporally controlling morphogen signaling within the embryo are still scarce. Here, we developed a photoactivatable Nodal receptor to determine how the temporal pattern of Nodal signaling affects cell fate specification during zebrafish gastrulation. By using this receptor to manipulate the duration of Nodal signaling in vivo by light, we show that extended Nodal signaling within the organizer promotes prechordal plate specification and suppresses endoderm differentiation. Endoderm differentiation is suppressed by extended Nodal signaling inducing expression of the transcriptional repressor *goosecoid* (*gsc*) in prechordal plate progenitors, which in turn restrains Nodal signaling from upregulating the endoderm differentiation gene *sox17* within these cells. Thus, optogenetic manipulation of Nodal signaling identifies a critical role of Nodal signaling duration for organizer cell fate specification during gastrulation.

INTRODUCTION

Nodal signals are members of the large family of transforming growth factor β (TGF-β) signals (Massagué, 2012) and play a pivotal role in the specification of the different germ layer progenitor cell types—ectoderm, mesoderm, and endoderm—during vertebrate gastrulation (Schier, 2003). In zebrafish and frogs, high Nodal signaling levels are generally believed to induce endoderm, whereas lower levels induce mesoderm (Schier, 2003; Schier and Talbot, 2005; Shen, 2007). These level-dependent effects of Nodal signaling are thought to be due to mesoderm transcriptional targets displaying high sensitivity to Nodal signaling, while endoderm targets are less responsive (Gurdon and Bourillot, 2001; Schier and Talbot, 2005). Considering that Nodal signals show locally restricted expression within the germ ring, a model has emerged wherein Nodal signals form a concentration gradient from the germ ring to the animal pole of the gastrula. This gradient in turn would provide positional information for cell fate specification, with cells close to the source of Nodal production becoming endoderm and cells further away mesoderm. More recent studies have suggested that not only the level, but also the duration of Nodal signaling are critical for mesoderm and endoderm cell fate specification (Gritsman et al., 2000; Gurdon and Bourillot, 2001; Hagos and Dougan, 2007; Rogers and Schier, 2011). This led to the cumulative dose model where the combination of signaling level and duration determines the dose upon which mesoderm and endoderm target genes are activated (Schier, 2009). In the framework of this model, also the specific kinetics of target gene induction—in particular the rate of gene transcription and the onset of induction—have recently been shown to modulate the precise spatial range of target gene expression within the embryo (Dubrulle et al., 2015). While the cumulative dose model provides a plausible mechanistic explanation for Nodal signals inducing mesoderm versus endoderm, important questions remain as to how the temporal pattern of Nodal signaling controls mesendoderm cell fate specification during gastrulation.

RESULTS

A recent observation using a transgenic reporter line to visualize endogenous Nodal signaling has suggested that a temporal window of Nodal signaling exists within the gastrulating zebrafish embryo determining the dimensions of the Nodal signaling domain (van Boxtel et al., 2015). Yet, how this temporal regulation of Nodal signaling translates in mesendoderm cell fate specification remains unclear. Previous studies have shown that the expression of Nodal signals within the early embryo from late blastula to early gastrula stages (4–6 hours post fertilization [hpf]), the period during which Nodal signaling induces mesendoderm cell fates (Feldman et al., 1998; Hagos and Dougan, 2007; Schier and Talbot, 2005), is largely restricted to the germ

This is an open access article under the CC BY license (http://creativecommons.org/licenses/by/4.0/).

ring (Feldman et al., 1998; Rebagliati et al., 1998a; van Boxtel et al., 2015). Interestingly, Nodal signal expression within the germ ring starts first within the embryonic organizer (shield) at the dorsal germ ring (Feldman et al., 1998; Rebagliati et al., 1998a) and is maintained longest within prechordal plate progenitors internalizing from the shield (Rebagliati et al., 1998a). This suggests that Nodal signaling starts earlier and lasts longer within the shield and its derivatives compared to the remainder of the germ ring. To determine whether not only the duration but also the level of Nodal signaling might differ between the shield versus the rest of the germ ring, we turned to *Tg(mezzo:eGFP)* embryos, in which the expression of EGFP is controlled by the promoter of *mezzo*, a pan-mesendoderm marker gene and direct target of Nodal signaling (Poulain and Lepage, 2002). Using the accumulation of EGFP in *Tg(mezzo:eGFP)* embryos as a proxy of endogenous Nodal signaling levels in embryos from late blastula to early gastrula stages (4–6 hr hpf), we found an overall similar level of Nodal signaling in cells within the shield compared to more lateral regions of the germ ring (Figures 1A and 1B; Movies S1 and S2). Collectively, these observations suggest that during the period of mesendoderm cell fate specification, the duration of Nodal signaling, more than its level, is extended in the shield compared to the rest of the germ ring.

To understand how extended Nodal signaling duration within the shield relates to the induction of mesendoderm cell fate specification therein, we analyzed cell fate specification in anterior axial mesendoderm (prechordal plate [ppl]) cells internalizing at the shield and migrating toward the animal pole during gastrulation (Gritsman et al., 2000). To this end, we made use of *Tg(sox17:GFP; gsc:TurboRFP)* embryos expressing RFP under the control of the *goosecoid* (*gsc*) promoter as a readout of ppl specification (Figure 1C) (Schulte-Merker et al., 1994) and expressing GFP under the control of the *sox17* promoter as a readout of endoderm differentiation (Figure 1C) (Alexander and Stainier, 1999). By simultaneously analyzing GFP and RFP expression in individual ppl progenitors at early gastrulation, we found that the level of *gsc* expression inversely correlated with the level of *sox17* expression in these cells (Figures 1D and 1E; Movie S3). Moreover, we found that cells in the center of the ppl expressed both higher levels of *gsc* and lower levels of *sox17* than cells in the periphery of the ppl (Figure 1F; Movie S3). These findings point at the intriguing possibility that extended Nodal signaling duration within the shield and its derivatives lead to a simultaneous upregulation of *gsc* expression, promoting ppl specification, and downregulation of *sox17* expression, suppressing endoderm differentiation.

To go beyond correlative evidence and unravel the causative relationship between the duration of Nodal signaling and the induction kinetics and interaction of factors involved in mesendoderm diversification within the shield, we sought to develop a tool with which we could precisely control the duration of Nodal signaling in the embryo. Such tool would then allow us to determine the capacity of temporal patterned Nodal signaling in controlling mesendoderm cell fate diversification during gastrulation, thereby generating predictions of the temporal activity of endogenous Nodal signaling that in turn could be tested experimentally. To this end, we constructed a pair of photoactivatable Nodal receptors, Opto-acvr1b and Opto-acvr2b, which can be used to control Nodal signaling with light in the absence of ligand. Specifically, we fused the light-oxygen-voltage (LOV) domain of aureochrome1 from *Vaucheria frigida* (Takahashi et al., 2007), which dimerizes upon blue light stimulation (Toyooka et al., 2011), to the C-terminal ends of the intracellular domains of the Nodal receptors Acvr1b and Acvr2b and anchored them to the plasma membrane by a myristoylation motif (Figure 2A). This LOV domain has previously been shown to induce the activation of dimerizing receptors with light (Grusch et al., 2014). To determine to what extent these photoactivatable receptors can be used to control Nodal signaling within the embryo, we first analyzed their subcellular localization and ability to induce Nodal signaling upon exposure to light at a level that does not cause any obvious phototoxicity (Figures S1A–S1D). We found that in embryos injected with *opto-acvr1b/2b* mRNA at the one-cell stage, the receptors localized to the plasma membrane of all cells at blastula and gastrula stages (Figures S1E–S1H), the period during which endogenous Nodal signaling is thought to induce mesoderm and endoderm (Feldman et al., 1998; Schier and Talbot, 2005). Using phosphorylation of endogenous Smad2 and nuclear translocation of EGFP-Smad2 as readouts for active Nodal signaling, we further found significantly increased signaling levels in gastrula stage embryos expressing both Opto-acvr1b and Opto-acvr2b when exposed to light during blastula and early gastrula stages as opposed to embryos kept in the dark (Figures 2B–2D and S2). Next, we determined whether light-induced receptor activation can also trigger the transcription of Nodal target genes. Using *gsc* promoter activity as readout of Nodal-induced target gene transcription (Joore et al., 1996; Schier, 2003; Schier and Talbot, 2005), we found strongly elevated levels of GFP expression in Opto-acvr1b/2b expressing *gsc:GFP* transgenic embryos (Doitsidou et al., 2002) at the end of gastrulation raised in the presence of light as opposed to embryos kept in the dark (Figure 2E). This phenotype is highly reminiscent of embryos uniformly overexpressing Nodal signals or constitutively active receptors (Figure S3).

In order to manipulate Nodal signaling in the absence of endogenous signaling, we expressed Opto-acvr1b/2b in MZ*oep* mutant embryos, which are defective in receiving Nodal ligands (Gritsman et al., 1999; Gurdon and Bourillot, 2001; Schier and Talbot, 2005). Exposing those embryos to light from fertilization onward strongly upregulated the expression of the Nodal target genes *gsc* and *notail* (*ntl*), which normally are expressed at only very low levels in MZ*oep* embryos (Figure 2F) (Gritsman et al., 1999). To determine how the light-induced levels of Nodal signaling in MZ*oep* embryos compare to endogenous levels of Nodal signaling in wild-type embryos, we compared the ability of exogenous and endogenous Nodal signaling to activate the expression of luciferase driven by an activin response element (ARE). We found similar levels of luciferase activity in wild-type embryos at shield stage (6 hpf) compared to shield stage MZ*oep* mutant embryos expressing Opto-acvr1b/2b receptor in the presence of light (Figure 2G). To further test the kinetics of Nodal target gene induction by Opto-acvr1b/2b, we analyzed the temporal profile of endogenous *gsc* and *ntl* expression in Opto-acvr1b/2b-expressing MZ*oep* mutant embryos relative to the onset and termination of light exposure. When embryos were exposed to light for 1 hr between sphere and dome stages

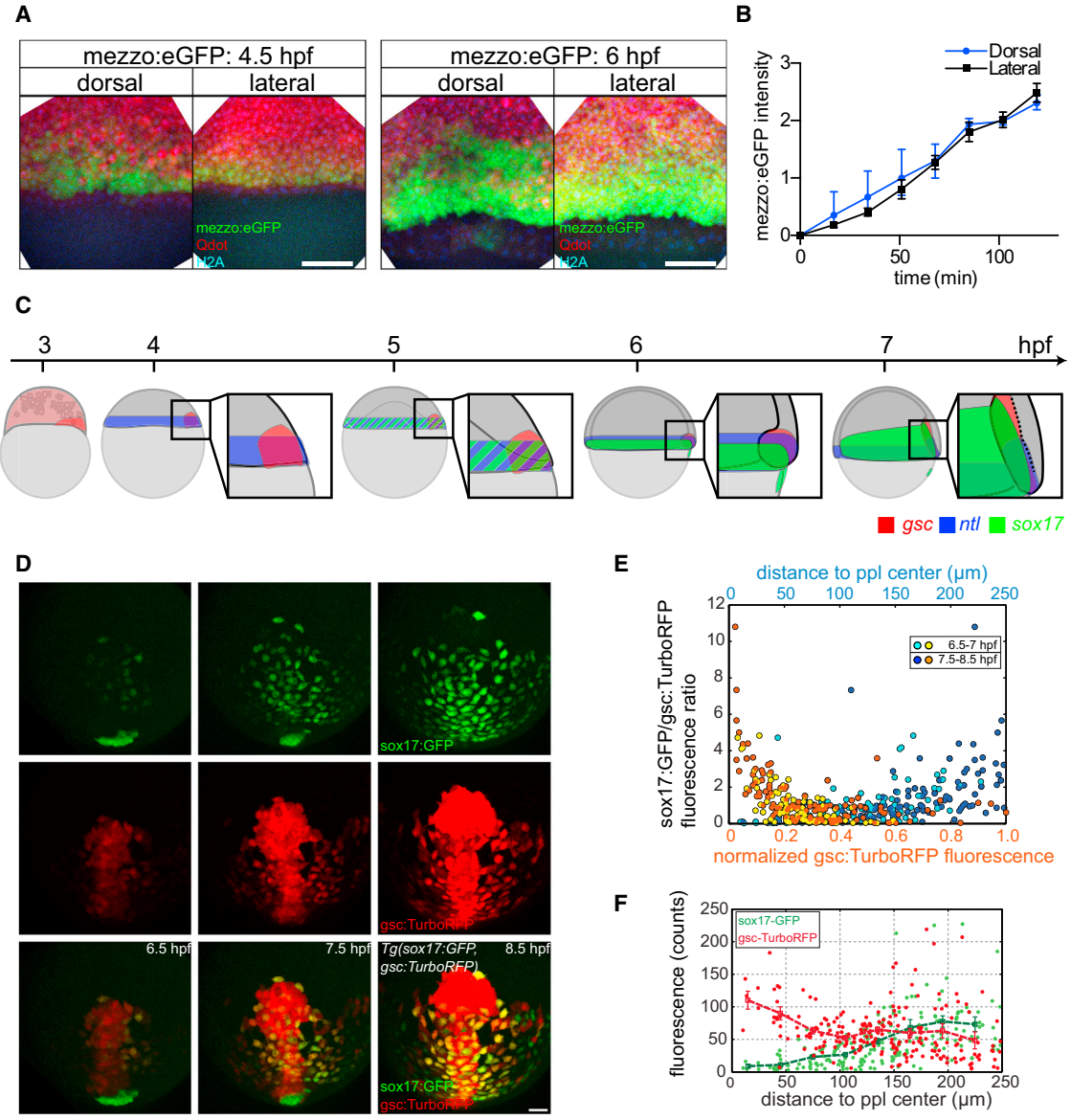

Figure 1. Temporal Nodal Signaling Activity and Cell Fate Specification

(A) Projection of image stacks showing *mezzo:eGFP* expression in the germ ring of *Tg(mezzo:eGFP)* embryos at 4.5 and 6 hpf injected with Qdots and expressing H2A-tagBFP to mark nuclei; dorsal and lateral views. Scale bar, 100 μm.

(B) Relative intensity of *mezzo:eGFP* in *Tg(mezzo:eGFP)* embryos at dorsal (blue line) and lateral side (black line) of the germ ring from 4.5–6.5 hpf; n = 3 embryos each.

(C) Schematic illustration of cell fate specification in zebrafish embryos at blastula and gastrula stages (3–7 hpf). *gsc*, *ntl*, and *sox17* expression domains are shown in red, blue, and green, respectively; dorsal germ ring margin (shield) at 4–6 hpf is magnified in the boxed areas next to the illustrations of whole embryos; dorsal side is to the right.

(D) Projection of image stacks showing *sox17*:GFP and *gsc*:TurboRFP expression in *Tg(sox17:GFP;gsc:TurboRFP)* embryos at 6.5, 7.5, and 8.5 hpf. Scale bar, 50 μm.

(E) Ratio of single cell *sox17*:GFP/*gsc*:TurboRFP fluorescence intensity values as a function of either normalized TurboRFP fluorescence intensities (yellow and orange dots), or distance to the prechordal plate (ppl) center measured within a distance of 250 μm around the ppl center (light and dark blue dots) in *Tg(sox17:GFP; gsc:TurboRFP)* embryos between 6.5–8.5 hpf; data were pooled for different time spans of development with yellow and light blue = 6.5–7 hpf and orange and dark blue = 7.5–8.5 hpf; single cell *gsc*:TurboRFP fluorescence values on the x axis were normalized to the maximum average single cell fluorescence intensity at each selected time point; n = 4 embryos and n = 208 cells.

(F) Single cell *sox17*:GFP (green) and *gsc*:TurboRFP (red) fluorescence intensity values as a function of distance to the ppl center used for calculating the fluorescence ratio in (E); binned data are shown as green and red lines; error bar, mean ± SEM.

See also Movies S1, S2, and S3.

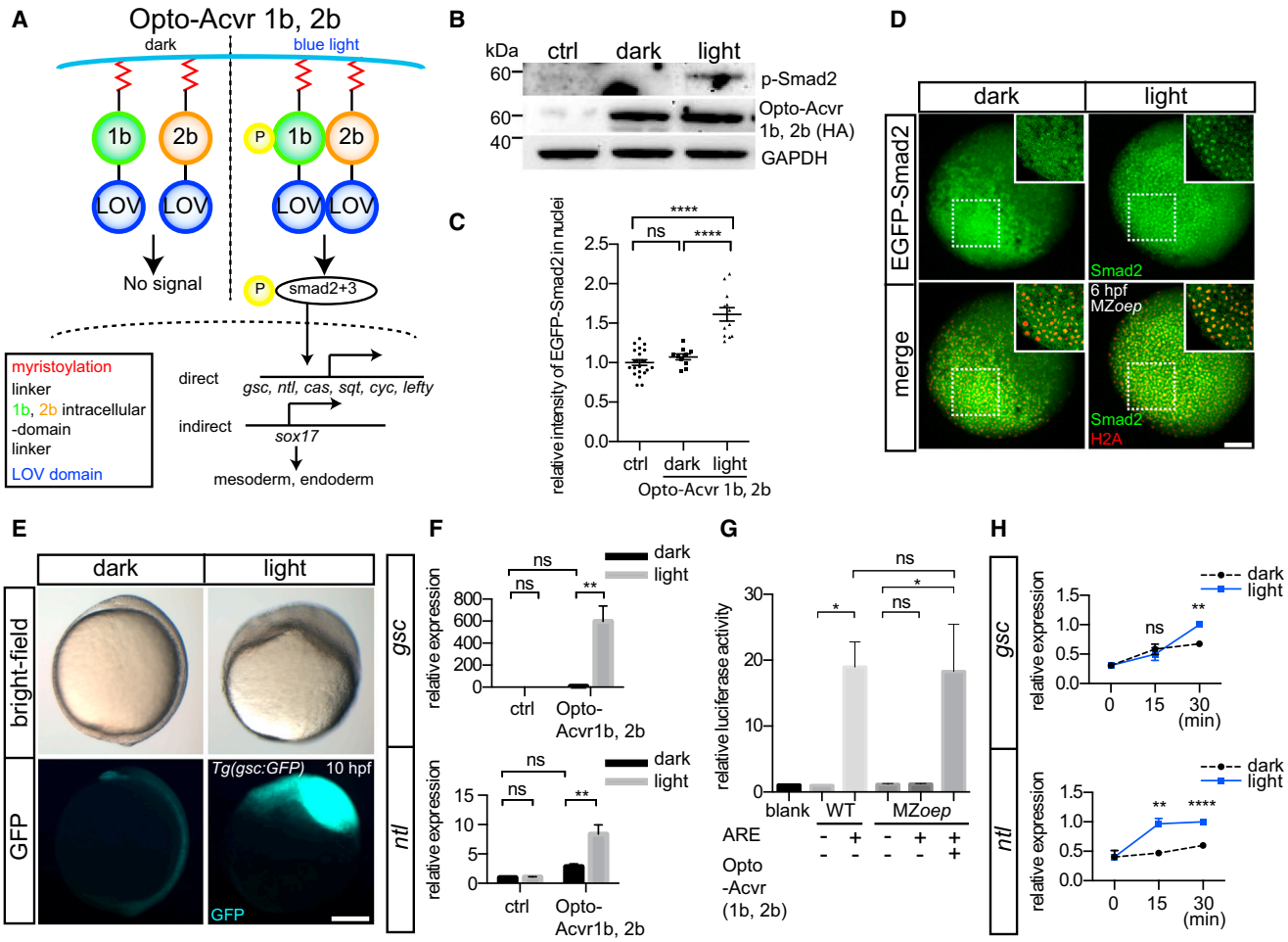

Figure 2. Construction and Validation of Photoactivatable Nodal Receptors

(A) Schematic illustration of the photoactivatable Nodal receptor constructs and their function; LOV domain is shown in blue, and intracellular domains of acvr1b and acvr2b are shown in green and orange, respectively; both receptors are anchored to the plasma membrane by a myristoylation motif shown in red; under blue light stimulation, the 1b and 2b receptors are dimerized, leading to the phosphorylation of smad2 and smad3 and activation of target gene expression.

(B) Western blot showing the expression of phosphorylated smad2, Opto-acvr1b, Opto-acvr2b, and GAPDH at dome stage (5 hpf) in MZ*oep* injected with *opto-acvr1b* and *opto-acvr2b* mRNA (20 pg each); water-injected embryos were used as controls (ctrl); embryos were exposed to light from high to dome stage (3–5 hpf).

(C) Quantification of nuclear EGFP-smad2 signal in shield stage (6 hpf) MZ*oep* embryos injected with *EGFP-smad2* (20 pg), *H2A-mCherry* (20 pg), and *opto-acvr1b* and *opto-acvr2b* mRNA (20 pg each) shown in (D); mean ± SEM; n (ctrl) = 22, n (dark) = 10, n (light) = 12 embryos; ANOVA test was used for the statistical evaluation with ****p < 0.0001; ns, not significant; MZ*oep* embryos injected with *EGFP-smad2* and *H2A-mCherry* mRNA only were used as ctrl.

(D) Projection of image stacks showing the localization of EGFP-smad2 in shield stage (6 hpf) MZ*oep* embryos injected with *EGFP-smad2* (20 pg), *H2A-mCherry* (20 pg), and *opto-acvr1b* and *opto-acvr2b* mRNA (20 pg each); animal pole views; embryos were exposed to blue LED light from high to shield stage (3–6 hpf); insets at the top right of each panel show single image planes of the boxed region in the main panel; EGFP-smad2 and H2A-mCherry are shown in green and red, respectively. Scale bar, 100 μm.

(E) *Tg(gsc:GFP)* embryos at bud stage (10 hpf) injected with *opto-acvr1b* and *opto-acvr2b* mRNA (20 pg each); embryos were exposed to blue LED light from two-cell to bud stage (0.5–10 hpf); upper panels are bright-field images and lower panels show *gsc*:GFP expression. Scale bar, 200 μm.

(F) Relative expression levels of *gsc* and *ntl* mRNA at shield stage (6 hpf) in MZ*oep* mutant embryos injected with *opto-acvr1b* and *opto-acvr2b* mRNA (20 pg each); embryos were exposed to light from two cell to shield stage (0.5–6 hpf); values are fold-induction compared to water-injected MZ*oep* mutant embryos kept in dark; mean ± SEM; independent triplicate experiments; ANOVA test was used for the statistical evaluation with **p < 0.01; ns, not significant.

(G) Quantification of luciferase activity induced by activin response element (ARE)-driven luciferase expression in wild-type (WT) and MZ*oep* mutant embryos injected with 3× ARE-lux plasmid (12.5 pg) and *opto-acvr1b* and *opto-acvr2b* mRNA (20 pg each); embryos were exposed to light from high to shield stage (3–6 hpf); values are fold-induction compared to water-injected WT ctrl embryos; mean ± SEM; independent triplicate experiments; ANOVA test was used for the statistical evaluation with *p < 0.05; ns, not significant.

(H) Relative expression levels of *gsc* and *ntl* mRNA at 5, 5.25 and 5.5 hpf in MZ*oep* embryos injected with *opto-acvr1b* and *opto-acvr2b* mRNA (20 pg each). Embryos were first exposed to light from sphere to dome stage (4–5 hpf) and then kept either in the dark or light for another 15 or 30 min; p values were determined between embryos kept in the dark and light at 15 and 30 min with t test; values are fold-induction over embryos at 5.5 hpf kept in the light; mean ± SEM; independent triplicate experiments; **p < 0.01; ns, not significant.

See also Figures S1, S2, and S3.

(4–5 hpf) and then either moved to the dark or kept in the light, we found a significant difference in the level of *gsc* and *ntl* expression between exposed versus unexposed embryos already 30 and 15 min after their separation, respectively (Figure 2H). This suggests that the activation-lifetime of Opto-acvr1b/2b with respect to its transcriptional output is <30 min and can be effectively used in early embryos for switching ectopic Nodal signaling on as well as off by termination of light exposure.

With this potent and reversible Opto-acvr1b/2b receptor in hand, we asked whether and how modulating the duration of Nodal signaling would affect mesendoderm specification. We first analyzed how the temporal pattern of uniform exogenous Nodal signaling activation in MZ*oep* embryos defective in endogenous Nodal signaling affects the induction kinetics and interaction of factors involved in mesendoderm diversification. We chose this reduced assay system as it allowed us to analyze the temporal aspect of Nodal signaling on target gene expression without interference from spatial and/or endogenous effects. When MZ*oep* embryos expressing Opto-acvr1b/2b were exposed to light during the first 6 hr (one-cell to shield stage) of development, the period during which mesoderm and endoderm are induced in the zebrafish embryo (Feldman et al., 1998; Schier and Talbot, 2005), the expression of *gsc* (ppl progenitors), *ntl* (pan-mesoderm), and *sox17* (endoderm) were upregulated (Figures 3A–3C and S4A; Table S1; for details of the endogenous expression domains see also Figure 1C). In contrast, restricted activation of Nodal signaling during the first 3 hr of development (one-cell to high stage) had little effect on the expression of these genes, while activation for the second 3 hr (high to shield stage) elicited the same response as continuous activation during the entire period (one-cell to shield stage; Figures 3A–3C and S4A; Table S1). These findings suggest that, consistent with previous observations (Hagos and Dougan, 2007), effective induction of mesoderm and endoderm cell fates requires Nodal signaling between high and shield stage (3–6 hpf).

We next evaluated whether further restricting the duration of Nodal signaling during this critical period of Nodal-mediated cell fate induction affects mesoderm and endoderm cell fate specification. We first verified that the levels of Nodal signaling elicited by activation of our Opto-acvr1b/2b receptors remained constant between high and shield stage (3–6 hpf) by analyzing ARE-induced luciferase expression when activating the receptor during the first (3–4 hpf), middle (4–5 hpf), and last (5–6 hpf) hr of the period. We found no significant differences in signaling levels between these different activation regimes (Figure S4B). We then analyzed whether a step-wise increase in the duration of Nodal signaling between high and shield stage (3–6 hpf) would affect the expression of genes involved in mesoderm and endoderm cell fate specification at shield stage (6 hpf). Interestingly, we found in line with previous observations (Dubrulle et al., 2015) that for *gsc* (ppl progenitors), there was only low-level induction after 1 hr (3–4 hpf) and 2 hr (3–5 hpf) activation, while after 3 hr of activation (3–6 hpf) the induction level was strongly increased (Figure 3B). For *ntl* (pan-mesoderm), the temporal activation pattern appeared similar to *gsc* although the increase after 3 hr of constant activation was less pronounced, likely due to high levels of *gsc* suppressing *ntl* expression (Artinger et al., 1997). Finally, *sox17* (endoderm) showed a completely different induction pattern from *ntl* and *gsc*, with low induction after 1 hr (3–4 hpf), very strong induction after 2 hr (3–5 hpf), and low induction again after 3 hr of activation (3–6 hpf; Figure 3C).

To determine whether this differential regulation of *gsc* versus *sox17* expression is due to changes in the expression of those genes within individual cells and/or alterations in the number of cells expressing them, we analyzed the expression pattern of *gsc* and *sox17* by whole mount in situ hybridization of treated embryos. This analysis showed that for *gsc*, the size of its expression domain as well as the level of *gsc* expression within this domain increased from 2 hr (3–5 hpf) to 3 hr (3–6 hpf) activation of Nodal signaling (Figure 3D), while for *sox17*, the opposite effects were detected (Figure 3D). This suggests that increasing the duration of Nodal signaling affects both the number of cells expressing *gsc* and/or *sox17* as well as the level of *gsc* and/or *sox17* expression in those cells. To confirm this conclusion on a more quantitative level, we also performed fluorescence-activated cell sorting (FACS) of GFP-expressing cells obtained from MZ*oep;Tg(gsc:GFP)* embryos after activation of Nodal signaling for 2 hr (3–5 hpf) versus 3 hr (3–6 hpf). We found that not only the number of *gsc* expressing cells, but also the expression level of *gsc* per cell increased from 2 hr to 3 hr activation (Figure 3E), confirming the observations from our in situ expression analysis.

To determine whether this difference in *sox17* versus *gsc* and *ntl* expression at shield stage in response to temporally restricted Nodal signaling between 3 and 5 hpf was due to differences in the induction of their expression by Nodal signaling or, alternatively, due to differences in their mRNA stability, we again activated the receptor for 2 hr (3–5 hpf) but monitored expression levels directly at the end of activation (5 hpf) rather than 1 hr later as in the previous experiments (Figures 3A–3C). We found that *gsc* and *ntl* showed the same low expression levels when analyzed at 5 hpf compared to 6 hpf (Figures 3F, 3G, and S4C), suggesting that the low expression of *gsc* and *ntl* at shield stage is due to low induction by Nodal signaling between 3 and 5 hpf rather than rapid mRNA decay between 5 and 6 hpf. Surprisingly, we also found that the endoderm gene *sox17* showed much lower induction when monitored directly at the end of activation rather than 1 hr later (Figures 3F and 3G), suggesting that for strong upregulation of *sox17* expression, Nodal signaling must be on for 2 hr (3–5 hpf) and off for another hr (5–6 hpf).

To identify the mechanism(s) by which this temporal pattern of Nodal signaling regulates *sox17* expression, we analyzed the induction of *casanova* (*cas*/*sox32*), an upstream regulator of *sox17* expression (Kikuchi et al., 2001) and direct transcriptional target of Nodal signaling. Similar to *gsc*, *ntl*, and *sox17*, 2 hr activation of Nodal signaling (3–5 hpf) led to only low induction of *cas*/*sox32* expression when assayed at 5 hpf (Figure S4C). However, different from *gsc* and *ntl* but similar to *sox17*, *cas*/*sox32* expression was upregulated following an hour during which Nodal signaling was switched off (Figure S4C). Interestingly, *cas*/*sox32* expression was also upregulated after continuous 3 hr activation of Nodal signaling from 3–6 hpf (Figure S4C), different from *sox17*, which was only mildly upregulated in this activation regime (Figures 3G and S4C). Together, these findings suggest that for both *sox17* and its upstream regulator *cas*/*sox32* to be expressed at shield stage (6 hpf), Nodal signaling must be on

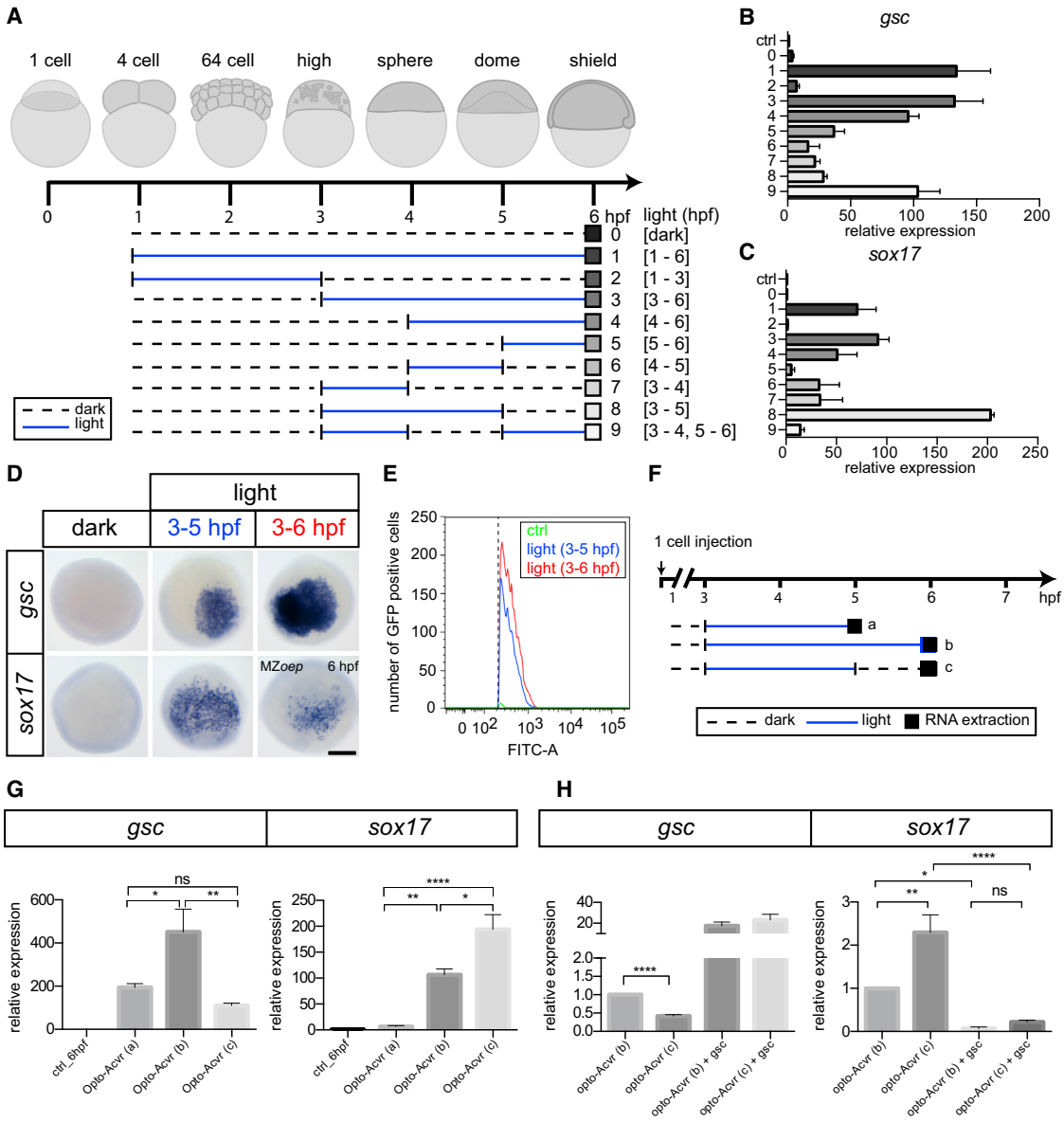

Figure 3. Temporally Patterned Nodal Signaling Activation and Cell Fate Specification

(A) Schematic illustration of temporally patterned blue LED light stimulation of Opto-acvr1b and 2b signaling; blue continuous lines indicate light stimulation (light), and black dashed lines indicate no stimulation (dark); mRNA expression analysis was done at 6 hpf (boxes).

(B and C) Relative expression levels of *gsc* (B) and *sox17* (C) mRNA in shield stage (6 hpf) MZ*oep* embryos injected with *opto-acvr1b* and *opto-acvr2b* mRNA (20 pg each) and exposed to blue LED light using the temporal patterns shown in (A); gene expression levels were quantified by qPCR; water-injected embryos were used as controls (ctrl); sample numbers correspond to the numbers of the different stimulation patterns shown in (A); values are fold-induction compared to ctrl embryos; mean ± SEM; independent triplicate experiments.

(D) Expression of *gsc* and *sox17* mRNA detected by whole-mount in situ hybridization in shield stage (6 hpf) MZ*oep* embryos injected with *opto-acvr1b* and *opto-acvr2b* mRNA (20 pg each); embryos were kept in the dark or activated with blue LED light from either high to dome stage (3–5 hpf) or high to shield stage (3–6 hpf); animal pole views. Scale bar, 200 μm.

(E) FACS analysis of MZ*oep;Tg(gsc:GFP)* embryos at shield stage (6 hpf) injected with *opto-acvr1b* and *opto-acvr2b* mRNA (20 pg each) and activated with blue LED light from either high to dome stage (3–5 hpf) or high to shield stage (3–6 hpf); non-injected embryos were used as ctrl; intensity of *gsc*:GFP and number of *gsc*:GFP positive cells were plotted on the x and y axes, respectively.

(F) Schematic illustration of temporally patterned blue LED light stimulation of Opto-acvr1b and Opto-acvr2b signaling; blue continuous lines indicate light stimulation (light), and black dashed lines indicate no stimulation (dark); black box marks time point of mRNA expression analysis.

(G) MZ*oep* embryos injected with *opto-acvr1b* and *opto-acvr2b* mRNA (20 pg each) were stimulated using the temporal patterns shown in (F); expression levels of *gsc* and *sox17* were determined by qPCR; water-injected embryos were used as ctrl; sample letters a–c correspond to the letters of the different stimulation patterns shown in (F); mean ± SEM; independent triplicate experiments, ANOVA test was used for the statistical evaluation with *p < 0.05, **p < 0.01, ****p < 0.0001; ns, not significant.

(legend continued on next page)

between 3 and 5 hpf, and subsequent upregulation of *sox17* but not *cas/sox32* is restrained by Nodal signaling between 5 and 6 hpf.

Gsc has previously been shown to function as a transcriptional repressor (Dixon Fox and Bruce, 2009; Latinkić et al., 1997). We thus hypothesized that Nodal-induced *gsc* expression at the onset of gastrulation (5–6 hpf) represses *sox17* expression, explaining why Nodal signaling must be switched off in this period for effective upregulation of *sox17*. To test this hypothesis, we determined how expression of ectopic *gsc* affects Nodal-induced *sox17* expression. To this end, we expressed ectopic *gsc* by injecting *gsc* mRNA at the one-cell stage and then analyzed how the induction of *sox17* at shield stage (6 hpf) by the 2 hr activation/1 hr inactivation regime used in the previous experiments is affected by ectopic *gsc*. Consistent with a repressor function of Gsc, the induction of *sox17* expression by Nodal signaling was strongly suppressed by ectopic *gsc* expression (Figure 3H). This supports the hypothesis that continuous Nodal signaling (3–6 hpf) restrains the upregulation of *sox17* expression between dome and shield stages (5–6 hpf) by inducing *gsc* expression during this period.

To determine whether Gsc can directly suppress *sox17* expression, we searched for the core recognition motifs of Gsc in the *sox17* promoter. Using the JASPAR core database, we found that Gsc-binding motifs are conserved from *Drosophila* to mice, suggesting that zebrafish Gsc might recognize similar motifs (Figure 4A). Analyzing the zebrafish *sox17* promoter revealed three potential Gsc binding sites (Figure 4B, P1–P3), two of which were located in a previously characterized repressor module (Figure 4B, P1, P2) (Chan et al., 2009). To determine whether Gsc binds to the *sox17* promoter, we performed chromatin immunoprecipitation (ChIP) experiments with FLAG-tagged Gsc and detected strong enrichment of Gsc on the *sox17* promoter (Figures 4C, 4D, S5A, and S5B). Next, we re-analyzed publicly available ChIP sequencing (ChIP-seq) data for H3 lysine 27 trimethylation (H3K27me3), a repressive chromatin mark, and H3 lysine 4 trimethylation (H3K4me3), an active chromatin mark (Pauli et al., 2012; Zhang et al., 2014), and found that the *sox17* promoter exhibited higher H3K27me3 level at dome (5 hpf) compared to shield stage (6 hpf; Figure 4E), consistent with the observation that endogenous *sox17* expression increases from dome to shield stage (Alexander and Stainier, 1999). ChIP analysis revealed that Gsc overexpression enhanced the trimethylation of H3K27 on the *sox17* promoter at shield stage (6 hpf; Figures 4F and S5C), suggesting that Gsc represses *sox17* promoter activity by enhancing the histone mark H3K27me3. Finally, to test whether Gsc suppresses the Nodal-induced expression of *sox17*, we analyzed the effect of ectopic expression of *gsc* on activation of the *sox17* promoter by the known upstream regulators Cas/sox32 (Kikuchi et al., 2001). To this end, we ectopically expressed a version of *cas/sox32* that is insensitive to negative regulation by the FGF/MAPK pathway (Poulain et al., 2006) either alone or together with *gsc*. We found that ectopic *gsc* expression effectively suppressed *cas/sox32*-induced *sox17* expression (Figures 4G and S5D), suggesting that *gsc* can directly suppress Cas/Sox32-induced activation of *sox17*.

Together, the results from our photoactivated Nodal signaling experiments support the plausibility of our original hypothesis that extended duration of Nodal signaling within the shield leads to upregulation of *gsc* and suppression of *sox17* expression in ppl progenitors therein (Figure 1) (Rebagliati et al., 1998a). To test how far the observations made by this ectopic Nodal signaling assay can be translated to the function of endogenous Nodal signaling within the germ ring, we first tested whether extending high Nodal signaling from late blastula to early gastrula stages would suppress *sox17* induction in endoderm cells of wild-type embryos. To this end, we uniformly activated Nodal signaling in Opto-acvr1b/2b expressing *Tg(sox17:GFP;gsc:TurboRFP)* embryos between 5–6.5 hpf—a condition that effectively upregulated *gsc* expression in our ectopic Nodal signaling assay system (Figures 3B and 3G)—and determined the number of *sox17*:GFP and *gsc:*TurboRFP expressing cells within the region of the ppl at 9 hpf. We found that activation of Nodal signaling from 5–6.5 hpf led to a concomitant increase in the number of *gsc* and decrease in the number of *sox17* expressing cells (Figures 5A–5C). This supports our hypothesis that extended duration of Nodal signaling represses *sox17* expression within the shield.

Next, we determined whether locally extending high Nodal signaling within the ventral germ ring margin from dome to 75% epiboly stage (5–8 hpf), a period during which the production of endogenous Nodal signals is already declining at this location (Rebagliati et al., 1998a), can trigger *gsc* expression similar to the situation within the shield. To this end, we temporally activated Nodal signaling in a locally restricted region within the ventral germ ring margin of Opto-acvr1b/2b expressing *Tg(gsc:GFP)* embryos from dome to 75% epiboly stage (5–8 hpf) and monitored the induction of GFP expression within this region. We found that cells within the activation region began to ectopically express GFP at the end of the activation period (Figure 5D; Movie S4), confirming our hypothesis that locally extended duration of Nodal signaling induces *gsc* expression.

Finally, we asked how Nodal signaling duration is extended within the shield compared to the rest of the germ ring. Given that *cyc* is strongly expressed in *gsc*-expressing ppl progenitors within the shield before and after internalization (Rebagliati et al., 1998a), and *cyc* mutants display a more prominent and penetrant defect in ppl formation than *sqt* mutants (Dougan et al., 2003; Rebagliati et al., 1998b), we speculated that extended duration of Nodal signaling within the shield is primarily due to persistent and high expression of *cyc* therein. To test this

(H) MZ*oep* embryos injected with *opto-acvr1b*, *opto-acvr2b* mRNA (20 pg each), and *gsc* mRNA (20 pg) were stimulated using the temporal pattern b or c shown in (F); expression levels of *gsc* and *sox17* were determined by qPCR at shield stage (6 hpf); values are fold-induction compared to *opto-acvr1b* and *opto-acvr2b* mRNA injected embryos stimulated using the temporal pattern b (3–6 hpf); mean ± SEM; independent quadruplicate experiments; for statistical evaluation t test was used for *gsc* expression (between temporal activation patterns b and c), and ANOVA test was used for *sox17* expression with *$p < 0.05$, **$p < 0.01$, ****$p < 0.0001$; ns, not significant.
See also Figure S4 and Table S1.

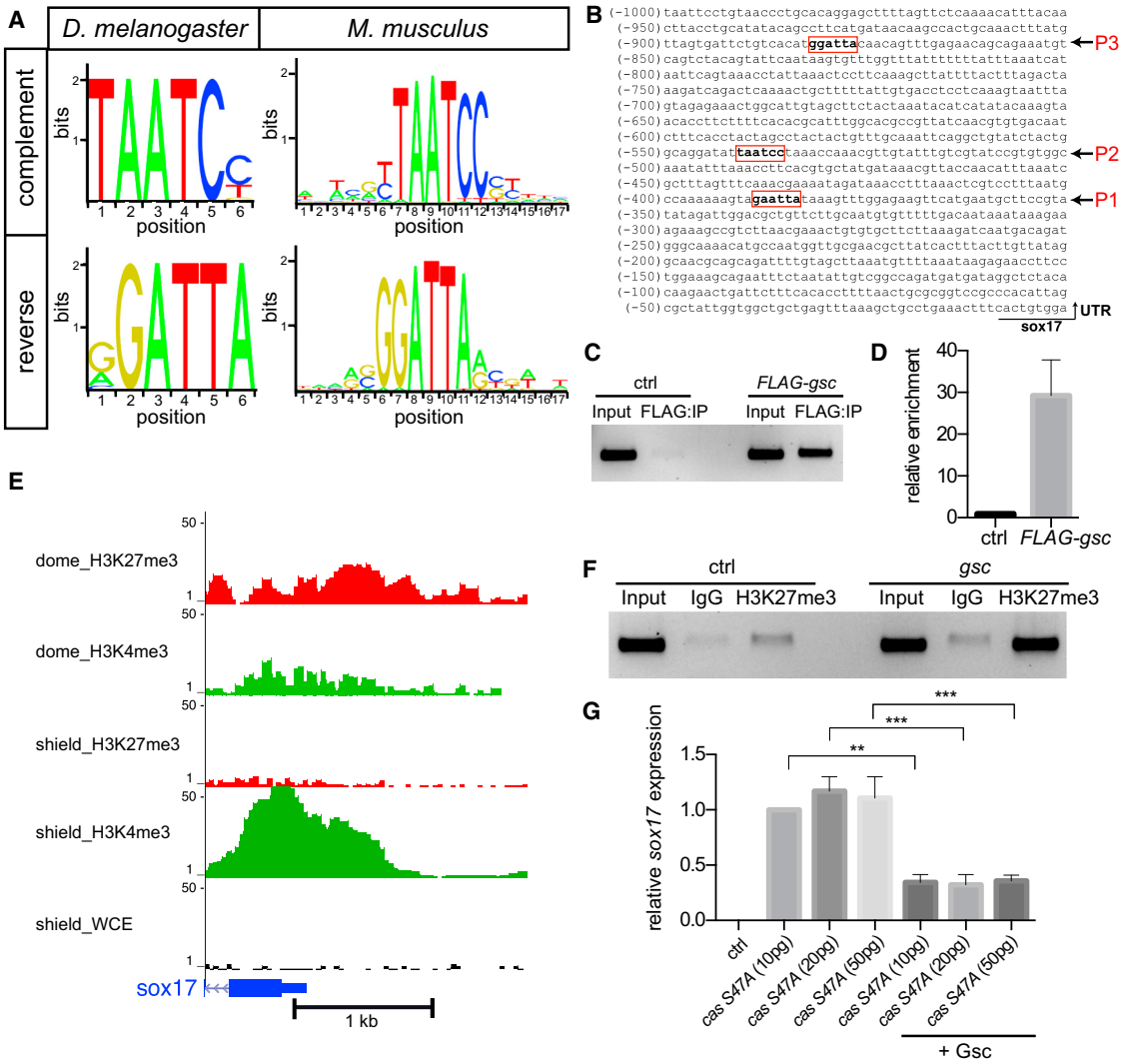

Figure 4. Suppression of *sox17* Expression by Gsc

(A) Core Gsc recognition motifs in *Drosophila melanogaster* and *Mus musculus*.

(B) In silico analysis for *sox17* promoter depicting multiple binding sites of Gsc on the upstream sequence of TSS region highlighted as red box, P1, P2, and P3.

(C) ChIP assay showing the occupancy of Flag-Gsc on the region of the *sox17* promoter (P2) in (B) in wild-type (WT) embryos injected with *Flag-gsc* (10 pg) mRNA; non-injected embryos were used as controls (ctrl); 1% input was used as a positive ctrl.

(D) Relative enrichment of Gsc for *sox17* promoter region shown in (C) quantified by qPCR; values are fold-induction compared to non-injected ctrl embryos; error bars show SE of two technical replicates in qPCR.

(E) UCSC browser view of ChIP seq reads for H3K27me3 (red) and H3K4me3 (green) in dome (5 hpf) and shield stage (6 hpf) embryos; whole cell extract (WCE) ctrl is shown for shield stage (6 hpf; black); *sox17* coding region is shown in blue.

(F) ChIP assay showing the differential occupancy of H3K27me3 in WT embryos injected with *gsc* mRNA (20 pg) at shield stage; non-injected embryos were used as ctrl; 10% input was used as a positive ctrl and IgG as a negative ctrl.

(G) MZ*oep* embryos injected with *cas S47A* (10, 20, 50 pg) and *gsc* mRNA (20 pg) were analyzed by qPCR for the expression level of *sox17* at shield stage (6 hpf); non-injected embryos were used as ctrl; values are fold-induction compared to embryos injected with 10 pg *cas S47A* mRNA; mean ± SEM, independent triplicate experiments; ANOVA test was used for the statistical evaluation with $^{**}p < 0.01$, $^{***}p < 0.001$.

See also Figure S5.

possibility, we globally interfered with *cyc* expression by injecting previously characterized *morpholinos* directed against *cyc* (0.5 ng/embryo) (Karlen and Rebagliati, 2001) and analyzed the number of *sox17*:GFP and *gsc:*TurboRFP expressing cells within the region of the ppl at 8.5 hpf. We found, consistent with previous observations (Thisse et al., 1994), that interfering with *cyc* expression led to a concomitant decrease in the number of *gsc* and increase in the number of *sox17* expressing cells (Figures 5E–5G). This suggests that *cyc* is particularly important for extended duration of Nodal signaling within the shield and its derivatives, leading to the characteristic upregulation of *gsc* and downregulation of *sox17* therein.

DISCUSSION

Here, we demonstrate that the temporal pattern of Nodal signaling is a key factor determining organizer cell fate specification at the onset of gastrulation. Both endoderm and ppl specification have previously been proposed to require high doses of Nodal signaling (Schier et al., 1997). Our data suggest that the duration of Nodal signaling is critical for ppl versus endoderm specification: in the shield, where Nodal signaling starts earlier and lasts longer than in the remainder of the germ ring, signal-receiving cells are likely to become ppl rather than endoderm by expressing genes involved in both ppl specification and endoderm repression (Figure 5H). Notably, our analysis of ppl versus endoderm specification is based on the expression of genes demarcating these different cell types during gastrulation. Consequently, our experiments provide information about the role of Nodal signaling duration in specifying the pool of ppl versus endoderm progenitors, but not necessarily about the commitment of those cells to a specific cell fate or type during later stages of development.

Genetic repressor systems, similar to the one we identified within the embryonic shield where Gsc suppresses *sox17* expression, have been proposed before to function downstream of other morphogens, such as Shh (Balaskas et al., 2012). However, the induction kinetics and interactions of the participating factors in those systems have only begun to be elucidated. Interestingly, Gsc, in addition to suppressing *sox17*, has previously been shown to repress *ntl* expression (Artinger et al., 1997), suggesting that *gsc* not only suppresses endoderm but also non-ppl mesoderm specification. Yet, the induction kinetics of *ntl* in relation to Nodal signaling and *gsc* expression appear rather different from *sox17*: while *sox17* expression becomes rapidly upregulated once Nodal signaling is terminated (Figures 3C and 3G), no such instantaneous upregulation was observed for *ntl* (Figures S4A and S4C). This suggests that *ntl* is less sensitive to changes in Gsc expression than *sox17*, potentially due to *ntl* being a direct target of Nodal signaling and thus directly depending on input from Nodal signaling, while *sox17* is regulated by Nodal signaling only indirectly via *cas/sox32*.

Notably, while our study demonstrates that both endogenous and exogenous upregulation of *gsc* suppresses endoderm specification (Figures 3 and 4), *gsc* loss-of-function studies have yet failed to provide evidence for *gsc* playing a major role in mesoderm and and/or endoderm specification in zebrafish (Dixon Fox and Bruce, 2009; Seiliez et al., 2006). It is thus conceivable that *gsc* has a partially redundant function in this process, and other as yet unidentified transcriptional repressors might cooperate with *gsc* in suppressing endoderm specification.

The role of morphogen signaling molecules in the organization of cell fates in space and time during embryogenesis has been extensively studied over the last decades (Ashe and Briscoe, 2006). There is clear evidence that the signaling duration by morphogens, such as hedgehog and TGF-β signals, is important for cell fate specification in development (Briscoe and Thérond, 2013; Dessaud et al., 2007; Harfe et al., 2004; Sorre et al., 2014). Yet, specifically addressing the role of morphogen signaling duration in development remains challenging, as tools for precisely manipulating the duration of morphogen signaling within the developing organism still need to be developed. The photoactivatable Nodal receptor presented here provides a powerful and much sought-after optogenetic tool (Tischer and Weiner, 2014; Toettcher et al., 2011, 2013) to dissect the temporal aspect of morphogen signaling in cell culture systems and also within the physiological environment of the developing embryo.

EXPERIMENTAL PROCEDURES

Generation of Photoactivatable Opto-acvr1b and Opto-acvr2b Nodal Receptors

A myristoylation domain (MYR) and a hemagglutinin (HA)-epitope flanking XbaI-restriction sites were transferred from a photoactivatable receptor plasmid (Grusch et al., 2014) to *pCS2*$^+$ vector using PCR and BamHI and EcoRI restriction sites. A XbaI restriction site in *pCS2*$^+$ backbone was then removed using site-directed mutagenesis. Kinase domains (KD) of Activin receptor 1b and 2b were amplified from zebrafish embryo cDNA library using PCR and inserted into *pCS2*$^+$ using XbaI and SpeI restriction sites. The LOV domain from *V. frigida* aureochrome1 (Grusch et al., 2014; Takahashi et al., 2007) was inserted into those constructs by PCR using SpeI restriction sites for producing C-terminal fusion proteins (Figure 2A). Finally, glycine linker sequences (-GGGGSGGGGSGGGGS-) were inserted between the myristoylation and kinase domain and the kinase domain and LOV domain by PCR.

LED Light Activation of Opto-acvr1b and Opto-acvr2b Receptors

Embryos were stimulated by blue LED light using an incubator (Herp Nursery II, 69802, Lucky Reptile) equipped with 300 light-emitting diodes (SMD5050) (Grusch et al., 2014) and set to 28.5°C. Light intensity was controlled with an analog dimmer and measured with a digital power meter (PM100D; Thorlabs). Embryos were stimulated for the desired time interval with the maximal intensity of blue light (5.12 $\mu W/mm^2$) unless mentioned otherwise. For dark condition, embryos were kept in a light-tight box and raised in the same incubator as the light-exposed embryos. Embryo pictures were taken with a stereomicroscope (M165 FC, Leica).

Laser Activation of Opto-acvr1b and Opto-acvr2b Nodal Receptors

Two-cell stage embryos were mounted in an agarose mold using 0.2% low melting point agarose. The dish was mounted on a Leica SP5 upright confocal microscope equipped with a 25×/0.95 NA water-dipping lens (Leica). The entire microscope system was covered with a light-tight curtain to avoid light exposure from the outside. Embryos were kept in dark until the desired stage and then stimulated by light using a 458 nm laser. Embryos were stimulated every 65–70 s for 1.29 s with a radiant exposure of 0.30 $nJ/\mu m^2$. A 633 nm laser was used to record bright-field images of whole embryos. Spatial activation was performed using the region of interest (ROI) function.

Dual Color Time-Lapse Imaging of *Tg(sox17:GFP; gsc:TurboRFP)* Embryos

Embryos were mounted in an agarose mold using 0.5% low melting point agarose. The dish was mounted on a Leica SP5 upright confocal microscope equipped with a 25×/0.95 NA water-dipping lens (Leica). 488 nm and 561 nm lasers were used simultaneously to record GFP and TurboRFP fluorescence, respectively. The movies were used to measure the correlated spatiotemporal expression levels of *gsc*:TurboRFP and *sox17*:GFP in single progenitor cells. Cell outlines were manually selected in z stacks using Fiji (Schindelin et al., 2012). Average fluorescence intensities were simultaneously measured in both channels at the equatorial cross-section of selected cells in single z slices for specified time points of development. Analyzed cells were randomly selected within a distance of 250 μm around the prechordal plate and centroid positions of outlined cells were used to calculate their distance to the prechordal plate center in 2D projected images. Data were further analyzed and processed using custom-written algorithms in MATLAB (R2014a, MathWorks).

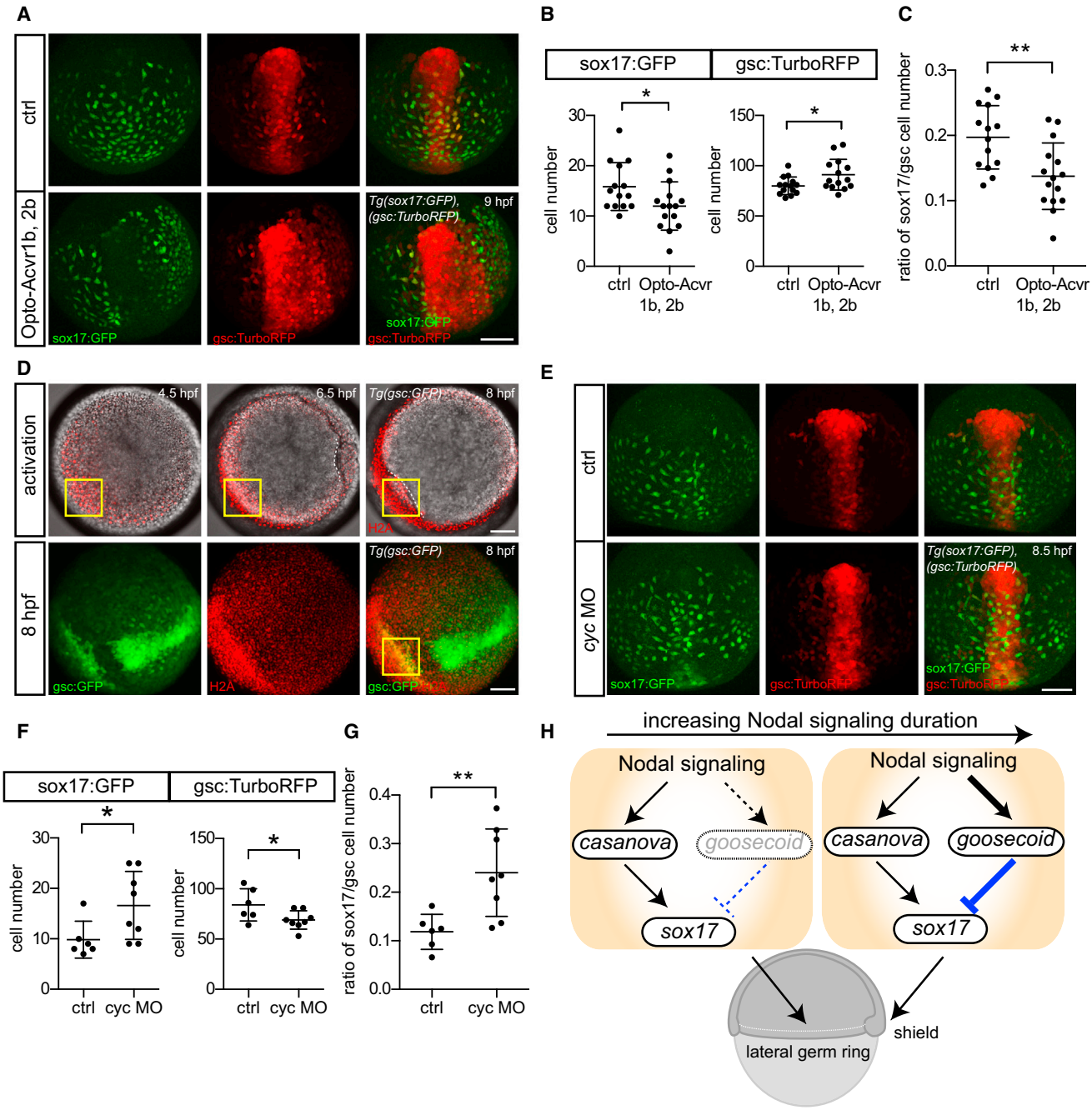

Figure 5. Endogenous Nodal Signaling Duration and Cell Fate Specification

(A) *sox17*:GFP and *gsc*:TurboRFP expression in *opto-acvr1b* and *opto-acvr2b* mRNA (20 pg each) injected *Tg(sox17:GFP;gsc:TurboRFP)* embryos at 90% epiboly stage (9 hpf); embryos were activated with blue LED from 5–6.5 hpf; dorsal views; water-injected embryos were used as controls (ctrl). Scale bar, 100 μm.

(B) Number of *sox17*:GFP and *gsc*:TurboRFP positive cells within the prechordal plate (ppl) region (200 μm^2 around the ppl center) for embryos shown in (A) at 9 hpf; n (ctrl) = 14, n (Opto-acvr1b, Opto-acvr2b) = 15 embryos; mean ± SD; t test was used for the statistical evaluation with $p^* < 0.05$.

(C) Ratio of *sox17*:GFP to *gsc*:TurboRFP expressing cells within the ppl region for embryos shown in (B) at 9 hpf; n (ctrl) = 14, n (Opto-acvr1b, Opto-acvr2b) = 15 embryos; ; mean ± SD; t test was used for the statistical evaluation with $^{**}p < 0.01$.

(D) Activation of ectopic *gsc*:GFP expression in *opto-acvr1b* and *opto-acvr2b* mRNA (20 pg each) and *H2A-mCherry* (20 pg) injected *Tg(gsc:GFP)* embryos at 4.5, 6.5, and 8 hpf; *gsc*:GFP in green and H2A-mCherry outlining nuclei in red; Nodal signaling was activated in a spatially restricted area (yellow box; 150 μm^2) within the ventral germ ring margin using a 458 nm laser from 4.5–8 hpf (top panels); dashed white lines indicate endogenous (top middle) and induced (top right) leading edge ppl cells; bottom panel shows image stack projections of *gsc*:GFP and mCherry (nuclei) expression in activated embryos at 8 hpf; animal pole view. Scale bar, 100 μm.

(legend continued on next page)

Analysis of Cell Fate Specification in *opto-acvr1b* and *opto-acvr2b* mRNA Injected or *cyc* Morphant *Tg(sox17:GFP; gsc:TurboRFP)* Embryos

cyc morpholino (0.5 ng/embryo) (Karlen and Rebagliati, 2001) or *opto-acvr1b* and *opto-acvr2b* mRNA (20 pg each) was injected into *Tg(sox17:GFP; gsc:TurboRFP)* embryos at the one-cell stage. For temporal activation of Opto-acvr receptors, embryos were stimulated with blue LED light from dome to shield stage (5–6.5 hpf). Embryos were imaged ~8.5–9 hpf after mounting in an agarose mold using a Leica SP5 upright confocal microscope equipped with a 25×/0.95 NA water-dipping lens (Leica). The pictures were used to analyze the expression of *gsc*:TurboRFP and *sox17*:GFP in single progenitor cells. Cells were automatically selected in 3D pictures with Imaris software (Bitplane) within a 200 μm^2 region around the ppl.

Analysis of *mezzo* Promoter Activity

Tg(mezzo:eGFP) (Ruprecht et al., 2015) embryos were injected with *histone-tagBFP* mRNA and qDots 625 ITK (A10200, Thermo Fisher Scientific) at the one-cell stage. Live imaging of either the dorsal or lateral germ ring was performed for 2 hr between 40% and 60% epiboly stage (4–6 hpf) using a Leica SP5 upright confocal microscope at 28.5°C. Images were subsequently processed using Imaris and custom MATLAB scripts. *Mezzo:eGFP* positive cells within a 200 μm wide area centered on either the dorsal or lateral side of the germ ring were analyzed. Cells around the margin and internalized cells were quantified for the time points before and after internalization, respectively. Imaris spots with a diameter of 15 μm were centered on the cell nucleus and the mean EGFP and qDot intensity for each spot was calculated. For each embryo, the increase of average EGFP to qDot ratio was used to estimate *mezzo* promoter activity.

SUPPLEMENTAL INFORMATION

Supplemental Information includes Supplemental Experimental Procedures, five figures, one table, and four movies and can be found with this article online at http://dx.doi.org/10.1016/j.celrep.2016.06.036.

AUTHOR CONTRIBUTIONS

K.S., H.J., and C.-P.H. developed and designed the project. K.S. performed most of the experiments. S.J.P. performed the ChIP experiments and in silico analysis. V.B. performed and analyzed the *Tg(mezzo:eGFP)* and FACS experiments, and generated the *Tg(gsc:TurboRFP)* fish line. A.I.P., P.M., V.R., and D.C. helped with experimental design and data analysis. S.G., H.J., and C.-P.H. supervised the project. K.S., H.J., and C.-P.H. wrote the manuscript.

ACKNOWLEDGMENTS

We are grateful to members of the C.-P.H. and H.J. labs for discussions, R. Hauschild and the different Scientific Service Units at IST Austria for technical help, M. Dravecka for performing initial experiments, A. Schier for reading an earlier version of the manuscript, K.W. Rogers for technical help, and C. Hill, A. Bruce, and L. Solnica-Krezel for sending plasmids. This work was supported by grants from the Austrian Science Foundation (FWF): (T560-B17) and (I 812-B12) to V.R. and C.-P.H., and from the European Union (EU FP7): (CIG-303564) to H.J. A.I.-P. is supported by a Ramon Areces fellowship.

Received: January 19, 2016
Revised: April 21, 2016
Accepted: June 5, 2016
Published: July 7, 2016

REFERENCES

Alexander, J., and Stainier, D.Y. (1999). A molecular pathway leading to endoderm formation in zebrafish. Curr. Biol. *9*, 1147–1157.

Artinger, M., Blitz, I., Inoue, K., Tran, U., and Cho, K.W. (1997). Interaction of goosecoid and brachyury in Xenopus mesoderm patterning. Mech. Dev. *65*, 187–196.

Ashe, H.L., and Briscoe, J. (2006). The interpretation of morphogen gradients. Development *133*, 385–394.

Balaskas, N., Ribeiro, A., Panovska, J., Dessaud, E., Sasai, N., Page, K.M., Briscoe, J., and Ribes, V. (2012). Gene regulatory logic for reading the Sonic Hedgehog signaling gradient in the vertebrate neural tube. Cell *148*, 273–284.

Briscoe, J., and Thérond, P.P. (2013). The mechanisms of Hedgehog signalling and its roles in development and disease. Nat. Rev. Mol. Cell Biol. *14*, 416–429.

Chan, T.-M., Chao, C.-H., Wang, H.-D., Yu, Y.-J., and Yuh, C.-H. (2009). Functional analysis of the evolutionarily conserved cis-regulatory elements on the sox17 gene in zebrafish. Dev. Biol. *326*, 456–470.

Dessaud, E., Yang, L.L., Hill, K., Cox, B., Ulloa, F., Ribeiro, A., Mynett, A., Novitch, B.G., and Briscoe, J. (2007). Interpretation of the sonic hedgehog morphogen gradient by a temporal adaptation mechanism. Nature *450*, 717–720.

Dixon Fox, M., and Bruce, A.E.E. (2009). Short- and long-range functions of Goosecoid in zebrafish axis formation are independent of Chordin, Noggin 1 and Follistatin-like 1b. Development *136*, 1675–1685.

Doitsidou, M., Reichman-Fried, M., Stebler, J., Köprunner, M., Dörries, J., Meyer, D., Esguerra, C.V., Leung, T., and Raz, E. (2002). Guidance of primordial germ cell migration by the chemokine SDF-1. Cell *111*, 647–659.

Dougan, S.T., Warga, R.M., Kane, D.A., Schier, A.F., and Talbot, W.S. (2003). The role of the zebrafish nodal-related genes squint and cyclops in patterning of mesendoderm. Development *130*, 1837–1851.

Dubrulle, J., Jordan, B.M., Akhmetova, L., Farrell, J.A., Kim, S.-H., Solnica-Krezel, L., and Schier, A.F. (2015). Response to Nodal morphogen gradient is determined by the kinetics of target gene induction. eLife *4*. http://dx.doi.org/10.7554/eLife.05042.

Feldman, B., Gates, M.A., Egan, E.S., Dougan, S.T., Rennebeck, G., Sirotkin, H.I., Schier, A.F., and Talbot, W.S. (1998). Zebrafish organizer development and germ-layer formation require nodal-related signals. Nature *395*, 181–185.

Gritsman, K., Zhang, J., Cheng, S., Heckscher, E., Talbot, W.S., and Schier, A.F. (1999). The EGF-CFC protein one-eyed pinhead is essential for nodal signaling. Cell *97*, 121–132.

Gritsman, K., Talbot, W.S., and Schier, A.F. (2000). Nodal signaling patterns the organizer. Development *127*, 921–932.

Grusch, M., Schelch, K., Riedler, R., Reichhart, E., Differ, C., Berger, W., Inglés-Prieto, Á., and Janovjak, H. (2014). Spatio-temporally precise activation of engineered receptor tyrosine kinases by light. EMBO J. *33*, 1713–1726.

(E) *sox17*:GFP and *gsc*:TurboRFP expression in *cyc* morphant (*cyc* MO) (0.5 ng/embryo) *Tg(sox17:GFP;gsc:TurboRFP)* at 80% epiboly stage (8.5 hpf); water-injected embryos were used as ctrl; dorsal views.
(F) Number of *sox17*:GFP and *gsc*:TurboRFP positive cells within the ppl region (200 μm^2 around the ppl center) for embryos shown in (E) at 8.5 hpf; n (ctrl) = 6, n (*cyc* MO) = 8 embryos; mean ± SD; t test was used for the statistical evaluation with *$p < 0.05$.
(G) Ratio of *sox17*:GFP to *gsc*:TurboRFP expressing cells within the ppl region for embryos shown in (F) at 8.5 hpf; n (ctrl) = 6, n (*cyc* MO) = 8 embryos; mean ± SD; t test was used for the statistical evaluation with **$p < 0.01$.
(H) Schematic illustration of changes in the induction of genes involved in mesendoderm cell fate specification as a function of endogenous Nodal signaling duration.
See also Movie S4.

Gurdon, J.B., and Bourillot, P.Y. (2001). Morphogen gradient interpretation. Nature *413*, 797–803.

Hagos, E.G., and Dougan, S.T. (2007). Time-dependent patterning of the mesoderm and endoderm by Nodal signals in zebrafish. BMC Dev. Biol. *7*, 22.

Harfe, B.D., Scherz, P.J., Nissim, S., Tian, H., McMahon, A.P., and Tabin, C.J. (2004). Evidence for an expansion-based temporal Shh gradient in specifying vertebrate digit identities. Cell *118*, 517–528.

Joore, J., Fasciana, C., Speksnijder, J.E., Kruijer, W., Destrée, O.H., van den Eijnden-van Raaij, A.J., de Laat, S.W., and Zivkovic, D. (1996). Regulation of the zebrafish goosecoid promoter by mesoderm inducing factors and Xwnt1. Mech. Dev. *55*, 3–18.

Karlen, S., and Rebagliati, M. (2001). A morpholino phenocopy of the cyclops mutation. Genesis *30*, 126–128.

Kikuchi, Y., Agathon, A., Alexander, J., Thisse, C., Waldron, S., Yelon, D., Thisse, B., and Stainier, D.Y. (2001). casanova encodes a novel Sox-related protein necessary and sufficient for early endoderm formation in zebrafish. Genes Dev. *15*, 1493–1505.

Latinkić, B.V., Umbhauer, M., Neal, K.A., Lerchner, W., Smith, J.C., and Cunliffe, V. (1997). The Xenopus Brachyury promoter is activated by FGF and low concentrations of activin and suppressed by high concentrations of activin and by paired-type homeodomain proteins. Genes Dev. *11*, 3265–3276.

Massagué, J. (2012). TGFβ signalling in context. Nat. Rev. Mol. Cell Biol. *13*, 616–630.

Pauli, A., Valen, E., Lin, M.F., Garber, M., Vastenhouw, N.L., Levin, J.Z., Fan, L., Sandelin, A., Rinn, J.L., Regev, A., and Schier, A.F. (2012). Systematic identification of long noncoding RNAs expressed during zebrafish embryogenesis. Genome Res. *22*, 577–591.

Poulain, M., and Lepage, T. (2002). Mezzo, a paired-like homeobox protein is an immediate target of Nodal signalling and regulates endoderm specification in zebrafish. Development *129*, 4901–4914.

Poulain, M., Fürthauer, M., Thisse, B., Thisse, C., and Lepage, T. (2006). Zebrafish endoderm formation is regulated by combinatorial Nodal, FGF and BMP signalling. Development *133*, 2189–2200.

Rebagliati, M.R., Toyama, R., Fricke, C., Haffter, P., and Dawid, I.B. (1998a). Zebrafish nodal-related genes are implicated in axial patterning and establishing left-right asymmetry. Dev. Biol. *199*, 261–272.

Rebagliati, M.R., Toyama, R., Haffter, P., and Dawid, I.B. (1998b). cyclops encodes a nodal-related factor involved in midline signaling. Proc. Natl. Acad. Sci. USA *95*, 9932–9937.

Rogers, K.W., and Schier, A.F. (2011). Morphogen gradients: from generation to interpretation. Annu. Rev. Cell Dev. Biol. *27*, 377–407.

Ruprecht, V., Wieser, S., Callan-Jones, A., Smutny, M., Morita, H., Sako, K., Barone, V., Ritsch-Marte, M., Sixt, M., Voituriez, R., and Heisenberg, C.-P. (2015). Cortical contractility triggers a stochastic switch to fast amoeboid cell motility. Cell *160*, 673–685.

Schier, A.F. (2003). Nodal signaling in vertebrate development. Annu. Rev. Cell Dev. Biol. *19*, 589–621.

Schier, A.F. (2009). Nodal morphogens. Cold Spring Harb. Perspect. Biol. *1*, a003459.

Schier, A.F., and Talbot, W.S. (2005). Molecular genetics of axis formation in zebrafish. Annu. Rev. Genet. *39*, 561–613.

Schier, A.F., Neuhauss, S.C., Helde, K.A., Talbot, W.S., and Driever, W. (1997). The one-eyed pinhead gene functions in mesoderm and endoderm formation in zebrafish and interacts with no tail. Development *124*, 327–342.

Schindelin, J., Arganda-Carreras, I., Frise, E., Kaynig, V., Longair, M., Pietzsch, T., Preibisch, S., Rueden, C., Saalfeld, S., Schmid, B., et al. (2012). Fiji: an open-source platform for biological-image analysis. Nat. Methods *9*, 676–682.

Schulte-Merker, S., Hammerschmidt, M., Beuchle, D., Cho, K.W., De Robertis, E.M., and Nüsslein-Volhard, C. (1994). Expression of zebrafish goosecoid and no tail gene products in wild-type and mutant no tail embryos. Development *120*, 843–852.

Seiliez, I., Thisse, B., and Thisse, C. (2006). FoxA3 and goosecoid promote anterior neural fate through inhibition of Wnt8a activity before the onset of gastrulation. Dev. Biol. *290*, 152–163.

Shen, M.M. (2007). Nodal signaling: developmental roles and regulation. Development *134*, 1023–1034.

Sorre, B., Warmflash, A., Brivanlou, A.H., and Siggia, E.D. (2014). Encoding of temporal signals by the TGF-β pathway and implications for embryonic patterning. Dev. Cell *30*, 334–342.

Takahashi, F., Yamagata, D., Ishikawa, M., Fukamatsu, Y., Ogura, Y., Kasahara, M., Kiyosue, T., Kikuyama, M., Wada, M., and Kataoka, H. (2007). AUREOCHROME, a photoreceptor required for photomorphogenesis in stramenopiles. Proc. Natl. Acad. Sci. USA *104*, 19625–19630.

Thisse, C., Thisse, B., Halpern, M.E., and Postlethwait, J.H. (1994). Goosecoid expression in neurectoderm and mesendoderm is disrupted in zebrafish cyclops gastrulas. Dev. Biol. *164*, 420–429.

Tischer, D., and Weiner, O.D. (2014). Illuminating cell signalling with optogenetic tools. Nat. Rev. Mol. Cell Biol. *15*, 551–558.

Toettcher, J.E., Voigt, C.A., Weiner, O.D., and Lim, W.A. (2011). The promise of optogenetics in cell biology: interrogating molecular circuits in space and time. Nat. Methods *8*, 35–38.

Toettcher, J.E., Weiner, O.D., and Lim, W.A. (2013). Using optogenetics to interrogate the dynamic control of signal transmission by the Ras/Erk module. Cell *155*, 1422–1434.

Toyooka, T., Hisatomi, O., Takahashi, F., Kataoka, H., and Terazima, M. (2011). Photoreactions of aureochrome-1. Biophys. J. *100*, 2801–2809.

van Boxtel, A.L., Chesebro, J.E., Heliot, C., Ramel, M.-C., Stone, R.K., and Hill, C.S. (2015). A Temporal Window for Signal Activation Dictates the Dimensions of a Nodal Signaling Domain. Dev. Cell *35*, 175–185.

Zhang, Y., Vastenhouw, N.L., Feng, J., Fu, K., Wang, C., Ge, Y., Pauli, A., van Hummelen, P., Schier, A.F., and Liu, X.S. (2014). Canonical nucleosome organization at promoters forms during genome activation. Genome Res. *24*, 260–266.